12th IFAC International Symposium on
Advanced Control of Chemical Processes
July 14-17, 2024. Toronto, Canada

Population Balance Model-based Dynamic Multiobjective Optimization of Yeast Cell Manufacturing ⋆

Krystian Ganko * **Marc D. Berliner** ** **Jinwook Rhyu** *
Liang Wu * **Richard D. Braatz** * **Sven Leyffer** ***

* *Department of Chemical Engineering, Massachusetts Institute of Technology, Cambridge, MA 02139 USA (e-mail: {kkganko; jrhyu; liangwu; braatz}@mit.edu)*
** *JuliaHub, Cambridge, MA 02139 USA (e-mail: marc.berliner@juliahub.com)*
*** *Mathematics and Computer Science Division, Argonne National Laboratory, Lemont, IL 60439 USA (e-mail: leyffer@anl.gov)*

Abstract: Biological systems play a key role in many advanced manufacturing processes, of which many have interesting nonlinear dynamics. We investigate a continuous yeast cell manufacturing process that produces sustained oscillations in outputs under nominal conditions. Using a population balance model to perform dynamic optimization with multiple objectives and observability constraints, we quantify tradeoffs on the Pareto surface for varying the extent of process oscillations that the decision-maker deems tolerable (or desirable). Numerical optimal control design for oscillatory distributed parameter systems is discussed within the context of both dynamic optimization and on-line nonlinear model predictive control strategies.

Keywords: Optimal control, distributed parameter system, population balance model, multiobjective optimization, biosystems and bioprocesses, chemical process control.

1. INTRODUCTION

Much of modern-day processing occurs in bioreactors, including in biofuel production (Aditiya et al. (2016)), wastewater treatment (Lee et al. (2017)), bulk and specialty chemicals manufacturing (Tejayadi and Cheryan (1995); Sharmila et al. (2020)), fermentation (Boulton and Quain (2001)), and biopharmaceutical production (Warnock and Al-Rubeai (2006); Tapia et al. (2016)). These dynamical systems require optimization and control to achieve stable, robust, and economically viable plant operation. Many of these systems exhibit nonlinear dynamics, complicating process operation with such phenomena as hysteresis, state multiplicity, and Hopf bifurcations (Lapidus and Amundson (1977); Strogatz (2015)).

This article considers the optimization and control of continuous yeast manufacturing. Yeast cells are used to produce a range of industrial products—from fermentation of small molecules in brewing and baking sectors to synthesis of complex therapeutics in the healthcare sector. An interesting aspect of the control of these manufacturing systems is that continuously cultured budding yeast produces sustained oscillations in cell densities and product titers when pushed into certain well-defined metabolic states (Kaspar von Meyenburg (1969, 1973); Strässle et al. (1989); Parulekar et al. (1986)). These oscillatory dynamics do not persist in traditional batch configurations. Moreover, studies have demonstrated that inducing oscillations in yeast cultures may yield, on average, higher quality and quantity products if coupled with periodic harvesting strategies (Hjortso (1996)). Despite these aspects and the fact that continuous manufacturing can improve costs, process controllability, and product quality over traditional batch processing (Sahlodin and Barton (2015)), batch mode operation has exclusively dominated at scale (Verbelen et al. (2006)).

To optimize continuous yeast manufacturing operation, this article considers measures of process oscillation that may be simultaneously optimized alongside economic objectives in a multi-objective formulation. In light of a product quality and/or quantity benefit from oscillatory operation, the decision-maker may consider leveraging oscillations in future continuous yeast manufacturing campaigns. Off-line computation of optimal control policies then becomes the backbone of re-computing oscillatory operating strategies. Herein, our main technical contribution is to present the numerical feasibility of model-based optimal control for an oscillatory distributed parameter system (DPS). Although others have studied model-based controller performance for this system, e.g., linear model predictive control (MPC) (Henson (2003)) and input-output linearization (Zhang and Henson (2001)), an optimal control study exploring the Pareto surface tradeoffs between tolerable degrees of process oscillation and economic profit has not yet been reported in the literature.

⋆ This work was supported by the U.S. Department of Energy, Office of Science, Office of Advanced Scientific Computing Research, Department of Energy Computational Science Graduate Fellowship under Award Number DE-SC0022158.

The work is organized as follows. Section 2 formulates the process and optimal control using a population balance model (PBM) and multiple competing objectives. Section 3 details the tools for numerical simulation and optimization to realize the multi-objective process. Section 4 demonstrates key tradeoffs and discusses the effects that oscillatory dynamics may have on optimal trajectories. Finally, Section 5 provides a perspective on how these results can be applied to on-line model-based control strategies.

2. PROCESS DESCRIPTION

Descriptions that follow are reproduced from other work by some of the authors (Inguva et al. (2023)) for clarity.

2.1 Model Formulation

Consider a continuously stirred bioreactor in which yeast is cultured in free suspension on a single substrate S. The reactor has no cell separation devices and gas phase dynamics are assumed to negligibly affect cellular growth. The reactor volume is assumed to be stabilized and kept approximately constant by a lower level control loop with dynamics that are faster than cell growth. All of these assumptions are reasonably accurate in a practical bioreactor equipment configuration.

Yeast cells in the reactor consume the substrate and progress through different growth states as quantified by their wet cell mass m: non-fissioning daughter cell ($m < m_{\mathrm{t}}^*$), non-fissioning mother cell with growing bud ($m_{\mathrm{t}}^* < m < m_{\mathrm{t}}^* + m_{\mathrm{a}}$), and mother cell with scissioning daughter cell bud ($m > m_{\mathrm{t}}^*$). The partitioning of mass between a budding daughter cell and a mother cell is asymmetric. An investigation of this system by Henson (2003) reported that oscillations are associated with interactions between the transition state mass m_{t}^* and critical fissioning mass m_{d}^* boundary movement as substrate concentrations change and yeast cell sub-populations synchronize.

The PBM for continuous culturing of yeast cells is given in (1)–(15). The hyperbolic partial differential equation (PDE) (1) has source terms for the birth, cleavage, and reactor outflow of yeast cells, typical of segregated cell, unstructured kinetics models (Fredrickson et al. (1967); Tsuchiya et al. (1966)). The yeast cell number distribution $N(m,t)$ is coupled to a substrate mass balance (7) and a filtered substrate S' response (9). The filtered substrate S' models a commonly observed delayed change in cell metabolism due to changes in extracellular substrate concentrations S. Movement in cell mass boundaries m_{t}^* and m_{d}^* is modeled as a linear dependence on filtered substrate.

Full specification of the model requires functions for the single-cell growth rate $k_{\mathrm{m}}(S')$, the fission rate $\Gamma_{\mathrm{m}}(m,S')$, the partition probability distribution $p(m,m',S')$, an initial yeast seed number distribution in mass $N_0(m,t)$, a boundary condition enforcing non-zero cell mass $N(0,t)$, and initial substrate concentrations $S(0)$ and $S'(0)$. The viable cell density (VCD) is equal to the zeroth-order moment $m_0(t)$ of the yeast population, and a differential equation for $m_0(t)$ as in (5) can be derived by integrating (1) over the cell mass m. Descriptions of model parameters and initial conditions are given in Table 1. More details are given by Zhang and Henson (2001) and Zhu et al. (2000).

$$\frac{\partial N(m,t)}{\partial t} + \frac{\partial [k_{\mathrm{m}}(S')N(m,t)]}{\partial m} = \Psi(m,t,N,S'), \tag{1}$$

$$\Psi(m,t,N,S') = 2\int_0^{m_{\max}} \Gamma_{\mathrm{m}}(m',S')p(m,m',m_{\mathrm{t}}^*)N(m',t)\mathrm{d}m' - [D+\Gamma_{\mathrm{m}}(m,S')]N(m,t), \tag{2}$$

$$N(m,0) = \frac{N_{00}}{\sigma_0\sqrt{2\pi}}\exp\left(\frac{-(m-\mu_0)^2}{2\sigma_0^2}\right) \sim \mathcal{N}\left(\mu_0,\sigma_0^2\right), \tag{3}$$

$$N(0,t) = 0, \tag{4}$$

$$\frac{\mathrm{d}m_0}{\mathrm{d}t} = -Dm_0 + \int_0^{m_{\max}} \Gamma_{\mathrm{m}}(m,S')N(m,t)\mathrm{d}m, \tag{5}$$

$$m_0(0) = N_{00}, \tag{6}$$

$$\frac{\mathrm{d}S}{\mathrm{d}t} = D(S_{\mathrm{f}} - S) - \frac{k_{\mathrm{m}}(S')}{Y}m_0, \tag{7}$$

$$S(0) = S_0, \tag{8}$$

$$\frac{\mathrm{d}S'}{\mathrm{d}t} = \alpha(S - S'), \tag{9}$$

$$S'(0) = S_0', \tag{10}$$

$$k_{\mathrm{m}}(S') = \frac{\mu_{\mathrm{m}}S'}{K_{\mathrm{m}} + S'}, \tag{11}$$

$$\Gamma_{\mathrm{m}}(m,S') = \begin{cases} 0 & \text{for } m \in \left[0, m_{\mathrm{t}}^* + m_{\mathrm{a}}\right) \\ \gamma e^{-\epsilon(m-m_{\mathrm{d}}^*)^2} & \text{for } m \in \left[m_{\mathrm{t}}^* + m_{\mathrm{a}}, m_{\mathrm{d}}^*\right] \\ \gamma & \text{for } m \in \left(m_{\mathrm{d}}^*, m_{\max}\right] \end{cases} \tag{12}$$

$$p(m,m',m_{\mathrm{t}}^*) = \begin{cases} Ae^{\left(-\beta(m-m_{\mathrm{t}}^*)^2\right)}\cdots & \text{for } (m<m') \wedge \cdots \\ + Ae^{\left(-\beta(m-m'+m_{\mathrm{t}}^*)^2\right)} & (m' > m_{\mathrm{t}}^* + m_{\mathrm{a}}) \\ 0 & \text{otherwise} \end{cases} \tag{13}$$

$$m_{\mathrm{t}}^*(S') = \begin{cases} m_{\mathrm{t}0} + K_{\mathrm{t}}(S_{\mathrm{l}} - S_{\mathrm{h}}) & \text{for } S' < S_{\mathrm{l}} \\ m_{\mathrm{t}0} + K_{\mathrm{t}}(S' - S_{\mathrm{h}}) & \text{for } S' \in [S_{\mathrm{l}}, S_{\mathrm{h}}] \\ m_{\mathrm{t}0} & \text{for } S' > S_{\mathrm{h}} \end{cases} \tag{14}$$

$$m_{\mathrm{d}}^*(S') = \begin{cases} m_{\mathrm{d}0} + K_{\mathrm{d}}(S_{\mathrm{l}} - S_{\mathrm{h}}) & \text{for } S' < S_{\mathrm{l}} \\ m_{\mathrm{d}0} + K_{\mathrm{d}}(S' - S_{\mathrm{h}}) & \text{for } S' \in [S_{\mathrm{l}}, S_{\mathrm{h}}] \\ m_{\mathrm{d}0} & \text{for } S' > S_{\mathrm{h}} \end{cases} \tag{15}$$

Table 1. Model variables and parameters, adapted from Zhang and Henson (2001).

Variable/ Parameter	Description	Initial/Nominal Values
N_{00}	Inoculum viable cell density	1×10^4 L^{-1}
μ_0	Inoculum mean cell mass	3×10^{-11} g
σ_0^2	Inoculum cell mass variance	1×10^{-22} g
S	Substrate concentration	25 g/L
S'	Filtered substrate	25 g/L
$D_{\max}$	Max dilution rate	0.5 hr^{-1}
$S_{\mathrm{f,max}}$	Max feed concentration	100 g/L
Y	Yeast to substrate yield	0.4 g
α	Metabolism adjustment rate	20 hr^{-1}
μ_{m}	Single cell growth rate	5×10^{-10} g/hr
K_{m}	Monod growth constant	2×10^{-11} g/L
γ	Maximum cell fission rate	200 hr^{-1}
ϵ	Fissioning inverse variance	5×10^{22} g^{-2}
m_{a}	Fissioning bud mass	1×10^{-11} g
A	Partitioning normalization	$\frac{5}{\sqrt{\pi}}\times10^{11}$ g^{-1}
β	Partitioning inverse variance	100×10^{22} g^{-2}
$m_{\mathrm{t}0}$	Minimal transition mass	6×10^{-11} g
K_{t}	Transition sensitivity to S'	1×10^{-13} g/g-L
S_{l}	Low substrate response limit	0.1 g/L
S_{h}	High substrate response limit	2 g/L
$m_{\mathrm{d}0}$	Minimal critical mass	11×10^{-11} g
K_{d}	Division sensitivity to S'	2×10^{-11} g/g-L
t_{f}	Full campaign time horizon	100 hr

2.2 Multiobjective Optimization Formulation

The nominal campaign manufacturing conditions simulated in this work produce oscillations in the on-line measured VCD titer m_0. These oscillations, which are considered detrimental to the process and product quality, arise from supercritical Hopf bifurcations in the PBM dynamics (Zhang and Henson (2001)). The objective is to design model-based optimal control policies in the dilution rate D and substrate feed concentration S_f for the full campaign manufacturing time horizon t_f that minimize oscillations while simultaneously maximizing economic objectives.

In continuous high cell density (HCD) yeast manufacturing, D and S_f regularly serve as manipulated variables with bounded actuator constraints D_max and $S_\mathrm{f,max}$, e.g., through a peristaltic pump or valve actuation and through ratio-controlled dilution of a high concentration feed stock, respectively (Westman and Franzén (2015); Gomar-Alba et al. (2015)). Other strategies potentially involving seed culture injections for direct cell population manipulation are unrealistic and difficult to control (Henson (2003)). Moreover, full state observability is often not available due to the challenge of maintaining sterile and calibrated on-line collection of cell number distributions through non-invasive optical imaging and/or biocapacitance sensors (Pais et al. (2020)).

Assuming that the yeast culture does not experience strong disturbances to its growth and metabolism during operation, three relevant performance objectives dependent on terminal time T are

$$J_1(T) = \int_0^T D(t) m_0(t) \mathrm{d}t, \tag{16}$$

$$J_2(T) = -\int_0^T D(t) S_\mathrm{f}(t) \mathrm{d}t, \tag{17}$$

$$J_3(T) = -\int_0^T \left(\frac{\mathrm{d}m_0}{\mathrm{d}t}\right)^2 \mathrm{d}t, \tag{18}$$

where J_1 is the economic gain due to continual cell titer harvesting, J_2 is the economic loss due to feed costs, and J_3 is the controller performance objective providing a measure of process oscillations. For input vector $\mathbf{u}(t) = [D(t), S_\mathrm{f}(t)]$, state vector $\mathbf{x}(t) = [S(t), S'(t), m_0(t)]$, and output vector $\mathbf{y}(t) = [S(t), m_0(t)]$,[1] a multi-objective optimal control problem (OCP) is

$$\begin{aligned} \max_{\mathbf{u}} \quad & \{J_1(t_\mathrm{f}), J_2(t_\mathrm{f}), J_3(t_\mathrm{f})\} \\ \text{s.t.} \quad & \text{model (1)–(15) on } \mathcal{D} = [0, m_\mathrm{max}] \times [0, t_\mathrm{f}], \\ & \mathbf{x}(t) \in \mathcal{X}, \quad \mathbf{x}(0) \in \mathcal{X}_0, \\ & \mathbf{u}(t) \in \mathcal{U}, \quad \mathbf{y}(t) \in \mathcal{Y}, \end{aligned} \tag{19}$$

where $\mathcal{X}$, $\mathcal{X}_0$, $\mathcal{U}$, and $\mathcal{Y}$ are predefined constraints on $\mathbf{x}$, $\mathbf{x}(0)$, $\mathbf{u}$, and $\mathbf{y}$, respectively. Next, we explore strategies for numerically solving this multi-objective OCP.

3. THEORY AND METHODS

The bioreactor model equations are non-dimensionalized to bring each system variable to be $\mathcal{O}(1)$ in magnitude. Importantly, non-dimensionalization improves the solution time and numerical precision of the simulations and optimal control calculations.

[1] The filtered substrate concentration S' is not observable.

3.1 Numerical Solution of the PBM

The PBM is highly nonlinear and tightly coupled to the evolution of substrate concentration $S(t)$, and it does not have an analytical solution. Obtaining reliable numerical optimal control profiles requires sufficiently accurate numerical resolution of the advection and source/sink term dynamics in the hyperbolic PDE. One approach is to use numerical Method of Lines (MOL) (Schiesser (1991)). MOL reduces the continuous cell mass dimension m, $N(m,t)$, and linear advection operator $\partial/\partial m$ to a finite-dimensional vector of mesh nodes $\mathbf{m} = [m_1, \ldots, m_{N_\mathrm{m}}] \in \mathcal{M} \subset \mathbb{R}^{N_\mathrm{m}}_{\geq 0}$, time-varying cell number density states $\mathbf{N}(t) = [N_1(t), \ldots, N_{N_\mathrm{m}}(t)] \in \mathcal{N} \subset \mathbb{R}^{N_\mathrm{m}}_{\geq 0}$, and finite advection operator $\mathbf{f}(\mathbf{m}, t, \mathbf{N}, S') : \mathcal{M} \times [0, t_\mathrm{f}] \times \mathcal{N} \times [0, S_\mathrm{f,max}] \to \mathbb{R}^{N_\mathrm{m}}$. Integral terms are discretized using the trapezoid rule with uniform mesh spacing Δm to obtain finite source/sink term operator $\mathbf{g}(\mathbf{m}, t, \mathbf{N}, S', D) : \mathcal{M} \times [0, t_\mathrm{f}] \times \mathcal{N} \times [0, S_\mathrm{f,max}] \times [0, D_\mathrm{max}] \to \mathbb{R}^{N_\mathrm{m}}$. Note the explicit dependence of the source/sink term operator on input $D(t)$.

These manipulations convert the PDE (1) into a system of coupled ordinary differential equations (ODEs) augmented by the S, S', m_0 state equations. That is, the state vector $\mathbf{x}$ is extended with $\mathbf{N}(t)$ to form $\tilde{\mathbf{x}} = [\mathbf{N}(t), S(t), S'(t), m_0(t)] \in \tilde{\mathcal{X}} \subset \mathbb{R}^{N_\mathrm{m}+3}_{\geq 0}$. Likewise, the finite advection and source/sink operators are extended into $\tilde{\mathbf{f}}(\mathbf{m}, t, \tilde{\mathbf{x}}, \mathbf{u})$ and $\tilde{\mathbf{g}}(\mathbf{m}, t, \tilde{\mathbf{x}}, \mathbf{u})$. Three advection operator discretizations are compared for accuracy and speed, including first-order upwind with finite difference method (FDM) ("Upwind FDM"); fifth-order weighted essentially non-oscillatory (WENO) Henrick-mapped scheme with FDM ("WENO FDM") (Hermanto et al. (2009); Gunawan et al. (2004); Jiang and Shu (1996); Henrick et al. (2005)); and eighth-order orthogonal collocation on finite elements ("OCoFE") (Finlayson (1980); Rice and Do (1991)). [2]

The Courant-Friedrichs-Lewy (CFL) number ν constraint is a necessary, but not sufficient, condition for numerically stable solution of the PBM using the MOL approach. For a discretized, first-order homogeneous hyperbolic PDE with advection coefficient $k_\mathrm{m}(S')$, uniform mesh spacing Δm, and constant time step Δt, the condition is that

$$\nu = \max\left\{\frac{k_\mathrm{m}(S')\Delta t}{\Delta m}\right\} \leq \nu_\mathrm{max}. \tag{20}$$

The maximal CFL number depends on the schemes used to discretize the advection operator and time derivative (Ketcheson (2009)). We use a restrictive CFL condition valid for the lowest order upwind scheme, or $\nu_\mathrm{max} = 1$. Because S' is bounded from above by $S_\mathrm{f,max}$, the above constraint implies an upper bound on the size of the time step for the MOL system to remain numerically stable,

$$\Delta t \leq \frac{\Delta m}{k_\mathrm{m}(S_\mathrm{f,max})} =: \Delta t_\mathrm{max}. \tag{21}$$

Inspection of the system separation of timescales showed that the resulting MOL ODE system is stiff. A fifth-order backward differentiation formula (BDF) time integrator from the CVODE solvers in the Sundials suite is chosen to

[2] Previous numerical solutions of (1)–(15) were carried out by Zhu et al. (2000) using OCoFE, which differs from other schemes in having a non-uniform grid and spectrally-accurate quadrature for the integral terms.

stably solve the stiff MOL system forward in time (Hindmarsh et al. (2005); Gardner et al. (2022); Hindmarsh et al. (2023)). For a sufficiently small time step size, this implicit linear multistep method holds strong stability-preserving (SSP) properties when used with Upwind FDM or WENO FDM. [3] Further inspection showed that the SSP time step size limit is larger than (21) and therefore not constraining.

3.2 Control Vector Parameterization

The OCP (19) is continuous and not analytically tractable. Control vector parameterization (CVP) (Schlegel et al. (2005)) is used to discretize the control input trajectories as piecewise-linear ("pwl") functions at K-many control elements uniformly partitioning the full campaign time horizon. This discretization induces $K+1$ control element boundary times $t_k \in [0, t_\mathrm{f}]$, where $k = 0, \ldots, K$. Each control element boundary has an associated control parameter $p_{j,k}$ for $j = 1, 2$, producing C^0 smooth input trajectories,

$$u_j(t) = \begin{cases} p_{j,0} & \text{for } t_0 = 0, \\ \frac{p_{j,k} - p_{j,k-1}}{t_k - t_{k-1}}(t - t_{k-1}) + p_{j,k-1} & \text{for } t \in (t_{k-1}, t_k]. \end{cases} \tag{22}$$

Time-explicit event functions are then used to step to and reinitialize the time integrator exactly [4] at $\{t_k\}$. Using the Leibnitz integral rule, the stage costs $j_1(t) = D(t)m_0(t)$, $j_2(t) = -D(t)S_\mathrm{f}(t)$, and $j_3(t) = -(\mathrm{d}m_0/\mathrm{d}t)^2$ are integrated together with the advection and source/sink terms as $\mathrm{d}J_l(t)/\mathrm{d}t = j_l(t)$, $J_l(0) = 0$ for $l = 1, 2, 3$. Applying the time integration operator $\mathbf{F}(\cdot)$, the OCP at discrete time points t_i for $i = 0, \ldots, N_\mathrm{t}$ becomes

$$\begin{aligned} \max_{\mathbf{p}} \quad & \{J_{1,N_\mathrm{t}}, J_{2,N_\mathrm{t}}, J_{3,N_\mathrm{t}}\} \\ \text{s.t.} \quad & \tilde{\mathbf{x}}_{i+1} = \mathbf{F}\Big(-\tilde{\mathbf{f}}(\mathbf{m}, t_i, \tilde{\mathbf{x}}_i, \mathbf{u}_i) + \tilde{\mathbf{g}}(\mathbf{m}, t_i, \tilde{\mathbf{x}}_i, \mathbf{u}_i)\Big), \\ & \mathbf{J}_{i+1} = \mathbf{F}(\mathbf{j}_i), \quad \tilde{\mathbf{x}}_0 = \tilde{\mathbf{x}}(0), \quad \mathbf{J}_0 = \mathbf{0}, \\ & \mathbf{0} \le \mathbf{p} \le \mathbf{p}_\mathrm{max}, \quad \mathbf{0} \le \tilde{\mathbf{x}}_i \le \tilde{\mathbf{x}}_\mathrm{max}, \quad \{t_k\} \subset \{t_i\}, \end{aligned} \tag{23}$$

where i subscripts denote evaluation at t_i, $\mathbf{J}(t)$ and $\mathbf{j}(t)$ concatenate $J_l(t)$ and $j_l(t)$, and the optimization algorithm solves for the decision variables $\mathbf{p} = [\mathbf{p}_1, \mathbf{p}_2] \in \mathcal{P} \subset \mathbb{R}^{2(K+1)}_{\ge 0}$. As $K \to \infty$, the discrete optimal input trajectory from the solution to (23) will approach the continuous optimal trajectory solution to (19).

3.3 Weighting Method, Warming, and Regularization

The (locally) Pareto optimal objective values $\mathbf{J}^* = [J_1^*, J_2^*, J_3^*]$ live in a set $\mathcal{J}^*$ that is defined as the subset of the boundary of the objective value space, $\partial\mathcal{J}$, for which all objectives cannot be simultaneously improved in any direction constrained to $\partial\mathcal{J}$ (Miettinen (1999)). The bioreactor dynamics are highly nonlinear so the Pareto surface for this set is expected to be non-convex and disjoint. A first pass to numerically compute the Pareto optimal set is to use the weighting method, which formulates a convex combination of the objectives. Using standard form and defining the direction of optimality to be $[-1, -1, -1]$ in the space $\mathcal{J}$, results in the weighting method formulation

$$\begin{aligned} \min_{\mathbf{p}} \quad & -w_1 J_{1,N_\mathrm{t}} - w_2 J_{2,N_\mathrm{t}} - w_3 J_{3,N_\mathrm{t}} \\ \text{s.t.} \quad & \text{conditions in (23)}, \quad w_1 + w_2 + w_3 = 1, \\ & w_1 \ge 0, \ w_2 \ge 0, \ w_3 \ge 0, \end{aligned} \tag{24}$$

which is solved at each admissible $\mathbf{w} = [w_1, w_2, w_3]$ to produce a corresponding $\mathbf{J}^*$ Pareto optimal point. The weighting method only uncovers convex portions of the Pareto optimal set. A more expensive but higher fidelity resolution of the Pareto optimal set would require using, e.g., the ϵ-constraint method (Miettinen (1999)).

A sufficiently high K is desirable to begin to match the period of the oscillatory response of the system. At higher control policy resolutions, Hopf bifurcation dynamics in the yeast system may be persistently excited. However, for entirely random initial guesses for $\mathbf{p}$, (23) becomes very difficult to converge at high CVP resolutions, i.e., $K \sim \mathcal{O}(100)$. Warm-starting is used, which involves taking previously converged K-element discrete optimal trajectories and bisecting them to form initial guesses for $2K$-element discrete optimal trajectories. Warming is restricted to the same $\mathbf{w}$ runs when solving (24).

Finally, it is common in numerical optimal control to reduce the non-unique family of discrete control policies solving (23) by penalizing abrupt changes in inputs between control elements (Schlegel et al. (2005); Nagy et al. (2005)). This regularization is added to the weighting method objective in (24) as the δ-weighted L_2-norm

$$\delta \left|\left| \frac{\mathrm{d}\mathbf{u}}{\mathrm{d}t} \right|\right|_2^2 = \delta \sum_{i=0}^{N_t} \sum_{j=1}^{2} \left(\frac{p_{j,k} - p_{j,k-1}}{t_k - t_{k-1}} \right)^2, \tag{25}$$

where the δ hyperparameter that least penalizes the Pareto optimal objective function set will vary along the Pareto surface. This motivated us to carry out a validation study at the nominal weighting $\mathbf{w} = [1/3, 1/3, 1/3]$, to find an optimal δ for regularization over the entire Pareto surface.

4. RESULTS AND DISCUSSION

4.1 Discretization Scheme Selection and Mesh Study

Fast and accurate solution of (1)–(15) is crucial to efficiently solve the high-dimensional OCP (23). As shown in Fig. 1 by the scaled cell number distribution at $t = 5.0$ hr, WENO FDM open-loop simulation is more numerically robust than both Upwind FDM and OCoFE for similar discretization resolutions. Although slower to simulate than Upwind FDM and OCoFE, [5] WENO FDM was selected as the advection operator discretization for solving (23). [6] Moreover, mesh study results given in Fig. 2 indicate that $N_\mathrm{m} = 300$ is the lowest resolution at which both numerical dispersion and state positivity violation are significantly reduced. All simulations are conducted in the

[3] SSP properties ensure monotonic decrease over time of a convex functional measure of the PDE solution spatial derivative over the domain $\mathcal{D}$. They are a generalization of the discrete total variation diminishing (TVD) property that numerically stable MOL solutions of the PBM necessarily satisfy (Ketcheson (2009); Lenferink (1991)).

[4] That is, within double precision.

[5] Median wall times for 100 runs using nominal conditions in Table 1: *Upwind FDM* ($N_\mathrm{m} = 300$), 304 ms; *WENO FDM* ($N_\mathrm{m} = 300$), 2278 ms; Zhu et al. (2000) *OCoFE* ($N_\mathrm{el} = 12$ and $N_\mathrm{col} = 8$), 339 ms; mesh-refined *OCoFE* ($N_\mathrm{el} = 32$ and $N_\mathrm{col} = 8$), 1191 ms.

[6] The OCoFE scheme at $N_\mathrm{el} = 12$ and $N_\mathrm{col} = 8$ used in past work (Zhang and Henson (2001); Zhu et al. (2000)) produced non-physical results due to Runge's phenomenon.

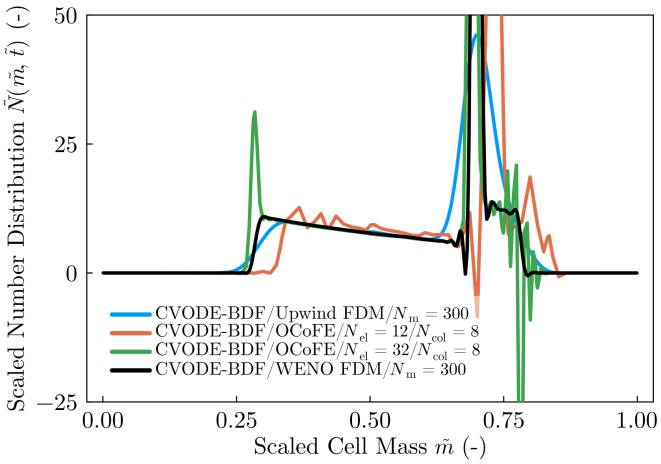

Fig. 1. At $t \approx 5.0$ hr, an abrupt substrate concentration depletion event destabilizes $N(m, t)$. During this transition, WENO FDM maintains state positivity better than OCoFE while mitigating numerical diffusion (i.e., smearing) better than Upwind FDM.

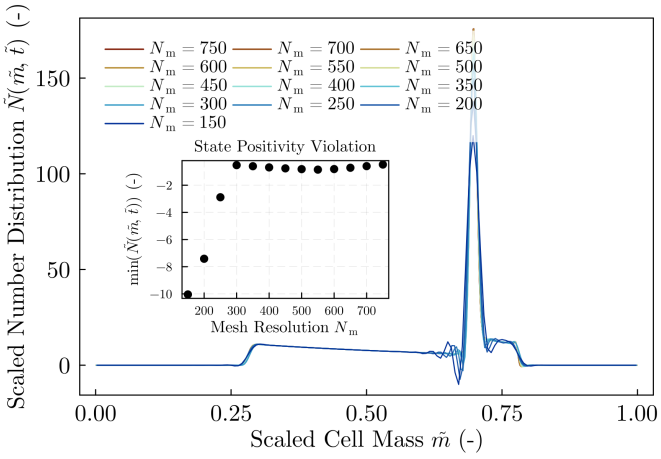

Fig. 2. Increasing mesh resolution in WENO FDM reduces numerical dispersion (i.e., spurious oscillation) at sharp spatial gradients, which is one of many features of WENO schemes (Jiang and Shu (1996)).

Julia programming language using DifferentialEquations.jl (Rackauckas and Nie (2017)) and Sundials.jl packages, and benchmarking is done using BenchmarkTools.jl.

4.2 Weighting Method Pareto Optimality

Formulation (19) penalized by (25) is at least once continuously differentiable with respect to the decision variables $\mathbf{p}$. This ensures that gradients of the objectives and constraints with respect to $\mathbf{p}$ are continuous, enabling low operational complexity, first-order optimization algorithms as an option for this system (Walkington (2023)). Instead, we used a second-order Sequential Least-Squares Quadratic Programming (SLSQP) method provided in the NLOPT.jl and Optimization.jl packages (Kraft (1994, 1988); Johnson (2007)) to reliably solve (24)–(25). In comparison to first-order methods, the SLSQP method converges in fewer iterations on local minima of (24) through the use of a Hessian approximation.

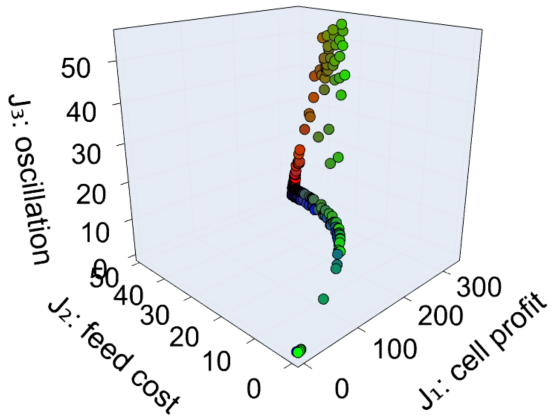

Fig. 3. The $\mathcal{J}$-space point cloud obtained from the solution of (24)–(25) for $K = 512$ warmed control trajectories using 228 $\mathbf{w}$ vectors. Red points map from $\mathbf{w}$ with the largest w_1, or more rewarding economic gains. Green points map from $\mathbf{w}$ with the largest w_2, or pricier feedstock. Blue points map from $\mathbf{w}$ with the largest w_3, or heavier penalization of process oscillations.

A δ validation study (results not shown) indicated that $\delta = 1.0$ adequately penalizes sharply changing input trajectories for the numerical OCP at $\mathbf{w} = [1/3, 1/3, 1/3]$. This study involved warming to optimal trajectories of $K = 1024$ elements. We then generated admissible $\mathbf{w}$ with an arbitrarily chosen resolution of 0.05 in each component w_i.[7] Finally, we solved (24)–(25) for each of the 228 $\mathbf{w}$ weighting vectors, aggregating the $\mathbf{J}$ results into a discrete point cloud. We show one perspective of this color-mapped, not entirely Pareto optimal set $\mathcal{J}^*$ in Fig. 3. The point cloud distribution suggests that: 1) control policies which produce large measures of process oscillations in continuous yeast manufacturing exist; 2) control policies producing these large oscillation measures may only be Pareto optimal when feedstock costs are high (i.e., when w_2 is large relative to w_1 and w_3); 3) solutions to (24)–(25) may not be converging to the true Pareto optimal control trajectories. This last suggestion is signaled by the mixed-color clustering in Fig. 3, where control trajectories are non-unique and insensitive to large variations in $\mathbf{w}$.

We emphasize that the convergence of solutions to the global minimum of (24)–(25) for each $\mathbf{w}$ *cannot* be guaranteed in polynomial time due to the non-convexity of the system. Moreover, solving the DPS (1)–(15) with numerical approximations to advection and source/sink operators corrupts the true topology of the objective space $\mathcal{J}$ with many non-physical local minima. For these poorly-conditioned, high-dimensional nonlinear programs, only rough heuristics (e.g., high total fractions of locally converged runs per batch, gradual changes in warming parameters, large numbers of SLSQP instantiations) are used in this work to approach globally optimal decision variable vectors $\mathbf{p}^*$. Specifically, converging to high K trajectories requires starting from $K = 2$ and applying the bisection strategy from Sec. 3. Refining to $\mathbf{p}^*$ at each K-element stage requires repeatedly applying biased Gaussian noise

[7] The map from $\mathbf{w}$ to the Pareto optimal set is unknown *a priori*. Otherwise, such a map may be inverted, assuming it is one-to-one, to grid $\mathbf{w}$ more efficiently.

of decreasing variance to each element of previous, locally optimal decision vectors $\mathbf{p}'$. This strategy generates structured $\mathbf{p}$ guesses which are more likely to converge to new, locally optimal $\mathbf{p}'$. [8]

Indeed, inspection of many of the clustered points in Fig. 3 indicated convergence to locally (not globally) optimal $\mathbf{p}'$ at early K, which resulted in non-unique and non-Pareto optimal $\mathbf{J}'$. Use of more conservative warming strategies, as well as multi-objective optimization methods capable of resolving the concavities of the Pareto front, would produce higher fidelity discrete representations of the Pareto front. These modifications would increase the already high, but off-line, costs of computing optimal control policies for continuous yeast manufacturing.

4.3 Excitation of Nonlinear Dynamics, and Tradeoffs

Despite these numerical challenges, several trajectories were sufficiently converged so as to be considered members of the Pareto surface. Verification of Pareto optimality for these few points is done using the ϵ-constraint method, which introduces nonlinear inequality constraints that can be *lifted* into the objective function through an L_2 penalty (see, e.g., Miettinen (1999) and Nocedal and Wright (2006)). The implementation will not be discussed here due to space constraints.

Two such Pareto optimal control policies are plotted in Fig. 4. These profiles show that the highest K-element trajectories are able to persistently excite the Hopf bifurcation dynamics of (1)–(15). As expected, oscillatory control policies are only optimal when the decision-maker deems process oscillations to be tolerable. This choice is encoded by decreasing w_3, or the weight on the "cost" of process oscillation. When the decision-maker views process oscillations as detrimental, w_3 may be increased and simpler control policies, such as operation at maximum actuation, are obtained.

Finally, we approximated total tradeoffs from the $\mathbf{J}^*$ values in Fig. 4 with

$$\Lambda_{n,m}(\mathbf{p}_1, \mathbf{p}_2) = \frac{J_n^*(t_\mathrm{f}; \mathbf{p}_1) - J_n^*(t_\mathrm{f}; \mathbf{p}_2)}{J_m^*(t_\mathrm{f}; \mathbf{p}_1) - J_m^*(t_\mathrm{f}; \mathbf{p}_2)}, \tag{26}$$

which compares Pareto optimal objectives between the oscillatory and non-oscillatory control policies $\mathbf{p}_1$ and $\mathbf{p}_2$, respectively (Miettinen (1999)). Equation (26) gives that

$$\Lambda_{1,2}(\mathbf{p}_1, \mathbf{p}_2) \approx +1.278, \tag{27}$$
$$\Lambda_{1,3}(\mathbf{p}_1, \mathbf{p}_2) \approx -1.322, \tag{28}$$
$$\Lambda_{2,3}(\mathbf{p}_1, \mathbf{p}_2) \approx -1.035, \tag{29}$$

indicating that oscillatory operation becomes more economical than non-oscillatory operation by reducing feed costs more than cell harvest profits are reduced. These tradeoffs align well with the observation in Fig. 3 that expensive feedstocks are a necessary condition for the appearance of large J_3 operating strategies. One practical implication may be that oscillating the dilution rate $D(t)$ in-phase with the yeast culture VCD oscillations will produce a less wasteful feeding strategy. More complete resolution of the Pareto surface will help ground these findings.

[8] With nine stages of K resolution, four levels of Gaussian noise variance, and 720 instantiations of SLSQP per stage-level, each $\mathbf{w}$ refinement process took 25920 instantiations of SLSQP, or roughly three hours of multithreaded computation on a 72-core server.

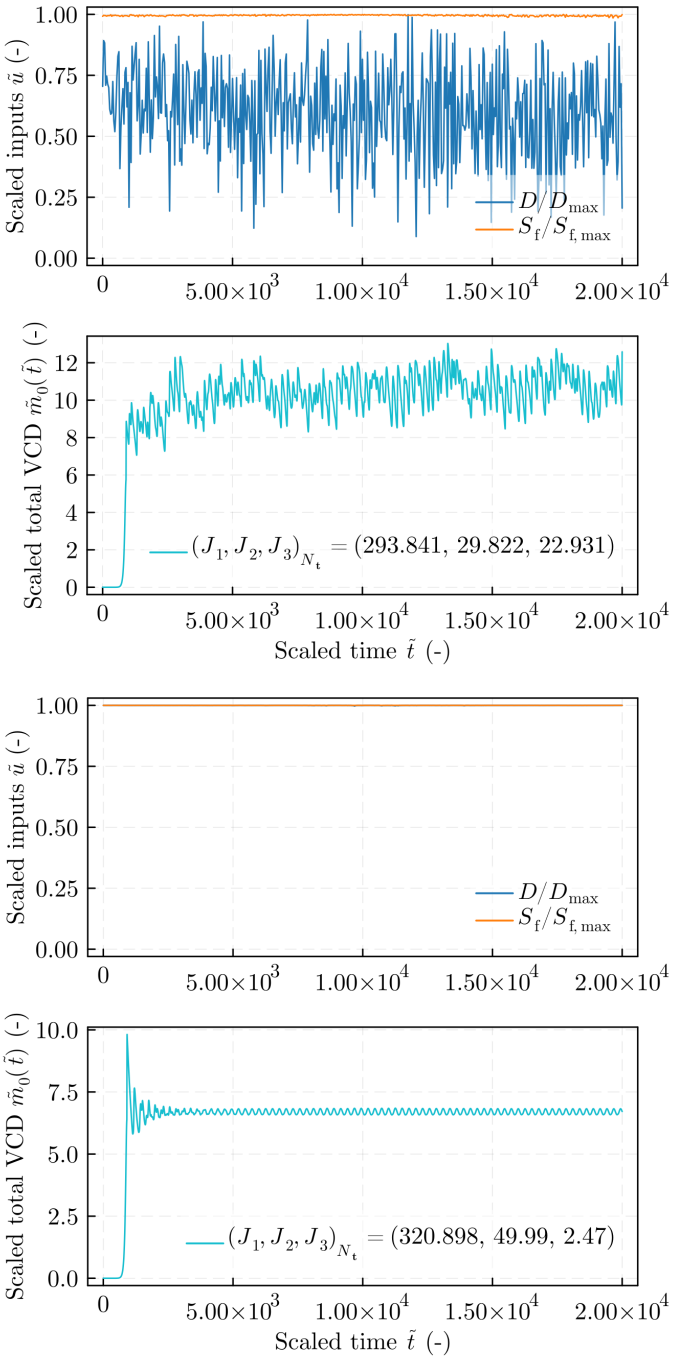

Fig. 4. Pareto optimal control policies and VCD m_0 responses for $K = 512$. (Top) The vector $\mathbf{w} = [0.2, 0.7, 0.1]$ admitted a high tolerance for process oscillations, while (Bottom) $\mathbf{w} = [0.45, 0.0, 0.55]$ admitted a low tolerance for process oscillations. Note that regardless of w_3, the optimal S_f control policy is to saturate for the entire campaign.

5. CONCLUSIONS AND FUTURE WORK

All discussions above are predicated upon a near-perfect model description of the yeast continuous manufacturing process. For biological systems, this is rarely the case.

The correction of model-plant mismatch by on-line optimal control tools, e.g., nonlinear MPC, can enable robust process operation and safety/quality constraint satisfaction in advanced manufacturing (Destro and Barolo (2022)). For the oscillatory DPS in this work, the implementation of MPC would be computationally expensive—as judged by the difficulty in converging the off-line numerical OCP—and reducing that computational cost is of interest.

Designing a stable economic MPC scheme for nonlinear and oscillatory systems requires carefully tuning the sampling time and prediction horizon. On one hand, the sampling time should be set small enough to capture model deviations and provide closed-loop performance that quickly attenuates oscillations in the controlled variables. On the other hand, a longer prediction horizon promotes closed-loop robustness, e.g., by inducing a larger region of stability and improving disturbance rejection. However, long-horizon MPC schemes have a high on-line computational cost, and shorter sampling times make it harder to converge the on-line optimization before needing to implement the next control action.

Some methods exist to alleviate the high on-line costs of long-horizon MPC schemes. For example, Lee and Lee (2001) describe the use of neuro-dynamic programming to approximate the cost-to-go function, which enables reducing a long-horizon problem to an equivalent short-horizon problem with a lower on-line computational cost. Zavala (2016) proposed a hierarchical MPC scheme to handle long-horizon MPC. Rao et al. (1998) adopted the discrete-time Riccati recursion in the interior-point framework to obtain a computational cost that scales linearly in the horizon length (as opposed to the cubic scaling of a naive approach). The differential dynamic programming (DDP)-based MPC methods of Tassa et al. (2014) extend the approach to nonlinear systems, preserving the linear complexity scaling in the prediction horizon length. Which method would work best for the yeast manufacturing system considered in this article is an open research question.

ACKNOWLEDGEMENTS

The authors thank Yingjie Ma, Prakitr Srisuma, and Tyler Chang for fruitful discussions on numerical optimization, optimal control formulations, and MPC applications.

REFERENCES

Aditiya, H., Mahlia, T., Chong, W., Nur, H., and Sebayang, A. (2016). Second generation bioethanol production: A critical review. *Renew. Sust. Energ. Rev.*, 66, 631–653. doi:10.1016/j.rser.2016.07.015.

Boulton, C. and Quain, D. (2001). Fermentation Systems. In *Brewing Yeast and Fermentation*, 260–376. Blackwell Science Ltd, Oxford, UK.

Destro, F. and Barolo, M. (2022). A review on the modernization of pharmaceutical development and manufacturing – Trends, perspectives, and the role of mathematical modeling. *Int. J. Pharm.*, 620, 1–26. doi:10.1016/j.ijpharm.2022.121715.

Finlayson, B.A. (1980). *Nonlinear Analysis in Chemical Engineering*. Ravenna Park Publishing, Seattle, WA.

Fredrickson, A.G., Ramkrishna, D., and Tsuchiya, H.M. (1967). Statistics and dynamics of procaryotic cell populations. *Math. Biosci.*, 1(3), 327–374. doi:10.1016/0025-5564(67)90008-9.

Gardner, D.J., Reynolds, D.R., Woodward, C.S., and Balos, C.J. (2022). Enabling New Flexibility in the SUNDIALS Suite of Nonlinear and Differential/Algebraic Equation Solvers. *ACM T. Math. Softw.*, 48(3), 1–24. doi:10.1145/3539801.

Gomar-Alba, M., Morcillo-Parra, M., and Olmo, M.d. (2015). Response of yeast cells to high glucose involves molecular and physiological differences when compared to other osmostress conditions. *FEMS Yeast Res.*, 15(5), fov039. doi:10.1093/femsyr/fov039.

Gunawan, R., Fusman, I., and Braatz, R.D. (2004). High resolution algorithms for multidimensional population balance equations. *AIChE J.*, 50(11), 2738–2749. doi:10.1002/aic.10228.

Henrick, A.K., Aslam, T.D., and Powers, J.M. (2005). Mapped weighted essentially non-oscillatory schemes: Achieving optimal order near critical points. *J. Comput. Phys.*, 207(2), 542–567. doi:10.1016/j.jcp.2005.01.023.

Henson, M.A. (2003). Dynamic modeling and control of yeast cell populations in continuous biochemical reactors. *Comput. Chem. Eng.*, 27(8), 1185–1199. doi:10.1016/S0098-1354(03)00046-2.

Hermanto, M.W., Braatz, R.D., and Chiu, M.S. (2009). High-order simulation of polymorphic crystallization using weighted essentially nonoscillatory methods. *AIChE J.*, 55(1), 122–131. doi:10.1002/aic.11644.

Hindmarsh, A.C., Brown, P.N., Grant, K.E., Lee, S.L., Serban, R., Shumaker, D.E., and Woodward, C.S. (2005). SUNDIALS: Suite of nonlinear and differential/algebraic equation solvers. *ACM T. Math. Softw.*, 31(3), 363–396. doi:10.1145/1089014.1089020.

Hindmarsh, A.C., Serban, R., Balos, C.J., Gardner, D.J., Reynolds, D.R., and Woodward, C.S. (2023). User Documentation for CVODE.

Hjortso, M.A. (1996). Population balance models of autonomous periodic dynamics in microbial cultures. Their use in process optimization. *Can. J. Chem. Eng.*, 74(5), 612–620. doi:10.1002/cjce.5450740510.

Inguva, P., Ganko, K., Dubs, A.B., and Braatz, R.D. (2023). Dynamics and Control of Oscillatory Bioreactors. *arXiv preprint arXiv:2306.15756*.

Jiang, G.S. and Shu, C.W. (1996). Efficient implementation of weighted ENO schemes. *J. Comput. Phys.*, 126(1), 202–228. doi:10.1006/jcph.1996.0130.

Johnson, S.G. (2007). The NLopt nonlinear-optimization package. URL `https://github.com/stevengj/nlopt`.

Kaspar von Meyenburg, H. (1969). Energetics of the budding cycle of Saccharomyces cerevisiae during glucose limited aerobic growth. *Arch. Mikrobiol.*, 66(4), 289–303. doi:10.1007/BF00414585.

Kaspar von Meyenburg, H. (1973). Stable Synchrony Oscillations in Continuous Cultures of Saccharomyces cerevisiae under Glucose Limitation. In B. Chance, A.K. Ghosh, E.K. Pye, and B. Hess (eds.), *Biological and Biochemical Oscillators*, 411–417. Academic Press, New York, NY.

Ketcheson, D.I. (2009). *High Order Strong Stability Preserving Time Integrators and Numerical Wave Propagation Methods for Hyperbolic PDEs*. Ph.D. dissertation, Dept. of Appl. Math., Univ. of Washington, Seattle, WA.

Kraft, D. (1988). *A software package for sequential quadratic programming*. DFVLR, Koln, Germany. Open Library ID: OL18926873M.

Kraft, D. (1994). Algorithm 733: TOMP–Fortran modules for optimal control calculations. *ACM T. Math. Softw.*, 20(3), 262–281. doi:10.1145/192115.192124.

Lapidus, L. and Amundson, N.R. (eds.) (1977). *Chemical Reactor Theory: A Review*. Prentice-Hall, Englewood Cliffs, NJ, 1 edition.

Lee, D.J., Jegatheesan, V., Ngo, H.H., Hallenbeck, P.C., and Pandey, A. (eds.) (2017). *Current Developments in Biotechnology and Bioengineering: Biological Treatment of Industrial Effluents*. Elsevier, Cambridge, MA, 1 edition.

Lee, J.M. and Lee, J.H. (2001). Neuro-dynamic programming method for MPC. *IFAC P. Vol.*, 34(25), 143–148. Publisher: Elsevier.

Lenferink, H.W.J. (1991). Contractivity-preserving implicit linear multistep methods. *Math. Comput.*, 56(193), 177–199. doi:10.1090/S0025-5718-1991-1052098-0.

Miettinen, K. (1999). *Nonlinear Multiobjective Optimization*. Kluwer Academic Publishers, Boston, MA.

Nagy, Z.K., Mahn, B., Franke, R., and Allgöwer, F. (2005). Nonlinear model predictive control of batch processes: An industrial case study. *IFAC P. Vol.*, 38(1), 1–6. doi:10.3182/20050703-6-CZ-1902.01576.

Nocedal, J. and Wright, S.J. (2006). Penalty and Augmented Lagrangian Methods. In T.V. Mikosch, S.I. Resnick, and S.M. Robinson (eds.), *Numerical Optimization*, Springer Series in Operations Research and Financial Engineering, 497–528. Springer, New York, NY. doi:10.1007/978-0-387-40065-5_17.

Pais, D.A.M., Galrão, P.R.S., Kryzhanska, A., Barbau, J., Isidro, I.A., and Alves, P.M. (2020). Holographic imaging of insect cell cultures: Online non-invasive monitoring of adeno-associated virus production and cell concentration. *Processes*, 8(4), 487. doi:10.3390/pr8040487.

Parulekar, S.J., Semones, G.B., Rolf, M.J., Lievense, J.C., and Lim, H.C. (1986). Induction and elimination of oscillations in continuous cultures of Saccharomyces cerevisiae. *Biotechnol. Bioeng.*, 28(5), 700–710. doi:10.1002/bit.260280509.

Rackauckas, C. and Nie, Q. (2017). DifferentialEquations.jl–a performant and feature-rich ecosystem for solving differential equations in Julia. *J. Open Res. Softw.*, 5, 15.

Rao, C.V., Wright, S.J., and Rawlings, J.B. (1998). Application of interior-point methods to model predictive control. *J. Optimiz. Theory Appl.*, 99, 723–757.

Rice, R.G. and Do, D.D. (1991). *Applied Mathematics and Modeling for Chemical Engineers*. John Wiley & Sons, Hoboken, NJ.

Sahlodin, A.M. and Barton, P.I. (2015). Optimal campaign continuous manufacturing. *Ind. Eng. Chem. Res.*, 54(45), 11344–11359. doi:10.1021/acs.iecr.5b01376.

Schiesser, W.E. (1991). *The Numerical Method of Lines: Integration of Partial Differential Equations*. Academic Press, San Diego, CA.

Schlegel, M., Stockmann, K., Binder, T., and Marquardt, W. (2005). Dynamic optimization using adaptive control vector parameterization. *Comput. Chem. Eng.*, 29(8), 1731–1751. doi:10.1016/j.compchemeng.2005.02.036.

Sharmila, V.G., Kavitha, S., Obulisamy, P.K., and Banu, J.R. (2020). Production of fine chemicals from food wastes. In *Food Waste to Valuable Resources*, 163–188. Elsevier, London, UK, 1st edition.

Strogatz, S.H. (2015). *Nonlinear Dynamics and Chaos With Applications to Physics, Biology, Chemistry, and Engineering*. CRC Press, Boca Raton, FL, 2 edition.

Strässle, C., Sonnleitner, B., and Fiechter, A. (1989). A predictive model for the spontaneous synchronization of Saccharomyces cerevisiae grown in continuous culture. II. Experimental verification. *J. Biotechnol.*, 9(3), 191–208. doi:10.1016/0168-1656(89)90108-9.

Tapia, F., Vázquez-Ramírez, D., Genzel, Y., and Reichl, U. (2016). Bioreactors for high cell density and continuous multi-stage cultivations: options for process intensification in cell culture-based viral vaccine production. *Appl. Microbiol. Biot.*, 100(5), 2121–2132. doi:10.1007/s00253-015-7267-9.

Tassa, Y., Mansard, N., and Todorov, E. (2014). Control-limited differential dynamic programming. In *IEEE International Conference on Robotics and Automation*, 1168–1175.

Tejayadi, S. and Cheryan, M. (1995). Lactic acid from cheese whey permeate. Productivity and economics of a continuous membrane bioreactor. *Appl. Microbiol. Biot.*, 43(2), 242–248. doi:10.1007/BF00172819.

Tsuchiya, H.M., Fredrickson, A.G., and Aris, R. (1966). Dynamics of Microbial Cell Populations. In T.B. Drew, J.W. Hoopes, and T. Vermeulen (eds.), *Advances in Chemical Engineering*, volume 6, 125–206. Academic Press, Cambridge, MA, 1 edition.

Verbelen, P.J., De Schutter, D.P., Delvaux, F., Verstrepen, K.J., and Delvaux, F.R. (2006). Immobilized yeast cell systems for continuous fermentation applications. *Biotechnol. Lett.*, 28(19), 1515–1525. doi:10.1007/s10529-006-9132-5.

Walkington, N.J. (2023). Nesterov's Method for Convex Optimization. *SIAM Rev.*, 65(2), 539–562. doi:10.1137/21M1390037. Publisher: Society for Industrial and Applied Mathematics.

Warnock, J.N. and Al-Rubeai, M. (2006). Bioreactor systems for the production of biopharmaceuticals from animal cells. *Biotechnol. Appl. Bioc.*, 45(1), 1. doi:10.1042/BA20050233.

Westman, J.O. and Franzén, C.J. (2015). Current progress in high cell density yeast bioprocesses for bioethanol production. *Biotechnol. J.*, 10(8), 1185–1195. doi:10.1002/biot.201400581.

Zavala, V.M. (2016). New architectures for hierarchical predictive control. *IFAC-PapersOnLine*, 49(7), 43–48. Publisher: Elsevier.

Zhang, Y. and Henson, M.A. (2001). Bifurcation analysis of continuous biochemical reactor models. *Biotechnol. Progr.*, 17(4), 647–660. doi:10.1021/bp010048w.

Zhu, G.Y., Zamamiri, A., Henson, M.A., and Hjortsø, M.A. (2000). Model predictive control of continuous yeast bioreactors using cell population balance models. *Chem. Eng. Sci.*, 55(24), 6155–6167. doi:10.1016/S0009-2509(00)00208-6.